A journal for the publication of
original research in all branches of physics

www.publish.csiro.au/journals/ajp

Monte Carlo Transport Simulation Techniques for Stellarator Fusion Experiments

S. A. Dettrick,[A] *H. J. Gardner*[B] *and S. L. Painter*[B,C]

[A]Naka Fusion Research Establishment, Japan Atomic Energy Research Institute,
801–1 Mukoyama, Naka-machi, Naka-gun, Ibaraki-ken 311–0193, Japan.
email: dettrick@pt101.naka.jaeri.go.jp

[B]Plasma Physics Laboratory, Research School of Physical Sciences and Engineering,
Australian National University, Canberra, ACT 0200, Australia.
[C]Present address: Center for Nuclear Waste Regulatory Analyses,
Southwest Research Institute, San Antonio, Texas, USA.

Abstract

We describe an implementation of a particle orbit-following simulation approach to the Monte Carlo calculation of neoclassical transport coefficients which has been developed for application to the H-1NF Heliac. We compare and contrast some Monte Carlo transport coefficient estimators that can be used in such computer codes, from both physical and computational perspectives, and we make recommendations for their use. Transport coefficient calculations are performed for the H-1NF in conditions that will be available after the full National Facility upgrade.

1. Background

Plasma transport in toroidal magnetic devices is complicated by the magnetic geometry, by multiple physical timescales, and by nonlinear effects caused by collective particle motion and by interaction between the plasma and the background magnetic and electric fields. Necessarily, this problem must be broken down into components and regimes of interest. In this section we give a brief qualitative description of the processes responsible for the transport of quiescent plasmas in background magnetic fields, which are described by neoclassical transport theory, and which are simulated in the Monte Carlo code which is the subject of this paper. For more detail, and for descriptions of the other important transport processes caused by collective waves, instabilities of the plasma column, and stochasticity in the structure of the magnetic fields, we refer the reader to the literature.

In regimes of interest in toroidal plasma physics, the first adiabatic invariant (the magnetic moment) $\mu = mv_\perp^2/2B$ is always well conserved, and we can use this fact to perform a 'gyroaverage' over the Larmor gyration, yielding equations of motion for the centre of gyration. This notionally reduces a fast gyrating particle to a magnetic dipole with moment μ drifting in a background magnetic field. In the presence of cylindrically symmetric fields, these drifting dipoles

10.1071/PH98106

remain on concentric cylindrically symmetric surfaces, with the only radial motion
being caused by collisions, which allow particles to diffuse radially with a diffusion
step length equal to the Larmor radius. This is called classical transport.

In toroidally symmetric magnetic geometry, the toroidal component of the field
makes the magnetic field strength vary on a toroidal surface. Since the magnetic
fields are designed so that the field lines wind helically around the toroidal
surfaces, particles with zeroth order motion lying along the field line experience a
variation in the field strength, and for some particles the velocity parallel to the
field line $v_\parallel$ can go to zero and change sign at a certain value of B, i.e. where
$K = mv_\parallel^2/2 + mv_\perp^2/2 = \mu B$. Such particles are called trapped,* or bounce orbits,
and if they are unperturbed by collisions they will execute a periodic motion,
due to the conservation of the toroidal angular momentum. When projected in
a plane where the toroidal angle is constant, these periodic orbits are in the
shape of bananas and so they are also called banana orbits. Their radial orbit
width is larger than the gyroradius, and the collisional transport is enhanced in
a non-trivial way, due to contributions not only from the larger diffusive step
width, but also due to the collisional transition of particles between the trapped
and untrapped states. These new features are described by neoclassical transport
theory.

Neoclassical theory also describes quiescent plasma transport in toroidal systems
which are not toroidally symmetric such as the H-1NF Heliac, which is represented
in Fig. 1. In this figure a typical plasma is shown, winding about a central ring
conductor, and enclosed by the set of coils which produce the toroidal component
of the magnetic field. The H-1NF clearly does not have toroidal (i.e. rotational)
symmetry, although it does satisfy certain other symmetries (Dewar and Hudson
1997). In such devices the toroidal angular momentum is not conserved so that
the banana orbit is no longer closed and periodic. In this case the locus of the
banana orbit drifts analagously to the locus of the Larmor orbit (see Fig. 2),
and in all but the most advanced magnetic configurations the bananas may drift
directly out of the plasma. In some cases the banana centre follows a confined
periodic orbit called a superbanana, and diffusion with a step width equal to the
superbanana width can also occur. A more detailed description of orbit dynamics
in the H-1NF Heliac and the important mitigating effect of the electric field is
given by Dettrick *et al.* (1998*b*).

Four timescales thus enter the neoclassical transport description. The first
three, in increasing order, are the Larmor gyration time τ_L, the banana orbit
or 'bounce' time τ_B, and the superbanana orbit time τ_{sb}. There may typically
be several orders of magnitude between each of these timescales. The fourth
timescale, which alone is independent of the magnetic field, is the τ_{90} collision
time, which may be of the order of τ_L in the plasma edge, and orders of magnitude
higher than τ_{sb} in the plasma core. A goal of neoclassical transport theory is
to calculate the particle and energy confinement times of the plasma, which in
fusion conditions may well exceed τ_{90}. Thus a problem presents itself: how to
efficiently simulate a long time-scale process which is produced by three shorter
time-scale detailed processes.

---

* It is an idiosyncracy of the nomenclature that 'trapped' orbits are poorly confined, whereas
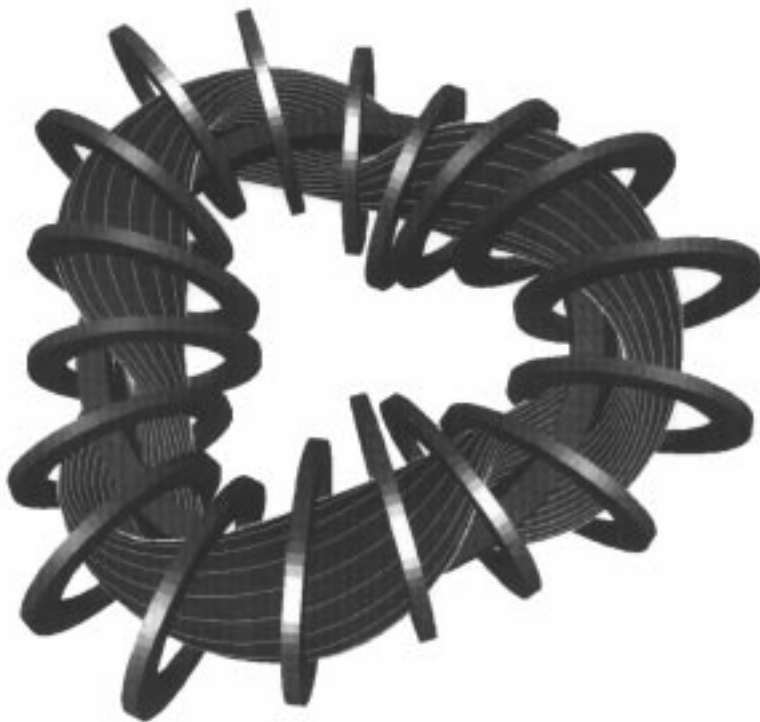'untrapped' orbits are well confined.

Fig. 1. Representation of the H-1NF Heliac. The plasma column is enclosed by a set of coils which provide the toroidal field (only half of these coils are shown here for clarity). The plasma winds three times about a central ring conductor which provides a poloidal magnetic field. A helical coil also winds three times about the ring conductor, and can be seen (in black) in the space between the plasma surface and the ring conductor. The white lines lying on the plasma surface represent magnetic field lines.

In Section 2 we describe our implementation of a particle orbit-following simulation approach to the calculation of neoclassical transport coefficients. In Section 3 we describe three statistical diagnostics from the literature which can be used to obtain transport measurements from such a code. We compare and contrast the results of these three diagnostics in Section 4. The computational requirements of the three are compared in Section 5, and further observations and conclusions are made in Sections 6 and 7.

2. Monte Carlo Transport Simulations

Monte Carlo transport codes follow many particles along their orbits, for several collision times, and calculate transport coefficients from the spatial evolution of the test particle distribution. The CPU time requirements are reduced by the use of gyro-averaged orbits, and in conditions where the second adiabatic invariant ($J = \oint m v_\parallel dl$ for banana orbits) is well conserved it is possible to further improve their efficiency by following the bounce averaged orbits. In H-1NF, however, this invariant is not well conserved in normal experimental conditions (Dettrick
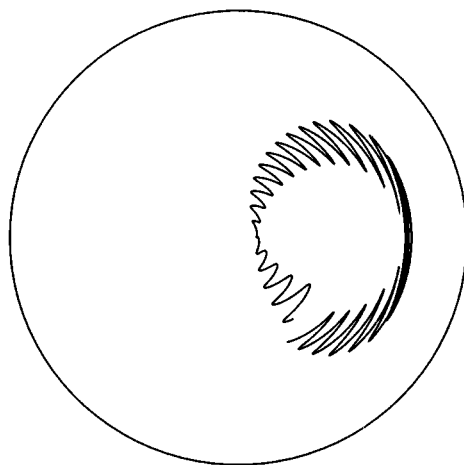
Fig. 2. A superbanana orbit in the H-1NF heliac, projected onto a plane of constant toroidal angle, in a coordinate system which renders the plasma cross section to be circular. The curve shown is the trajectory of the locus of the Larmor orbit (i.e. the gyro-orbit), and the extreme points of the oscillations in the curve are bounce points. Every triplet of consecutive bounce points demarcates an unclosed banana. The locus of the banana orbit can be seen to trace out a larger circle, which is the superbanana.

et al. 1998*b*) so in this paper we use the gyro-averaged, rather than the bounce averaged, equations of motion.

The interpretation of the results of Monte Carlo particle codes is problematic because of difficulties involved in the computation of the transport coefficients. The first (Potok *et al.* 1980; Boozer and Kuo-Petravic 1981; Mynick 1982) of these studies calculated diffusion coefficients. However, in the long mean free path regime the transport is dominated by direct losses, sustained by diffusion in velocity space which replenishes the loss cone. In these conditions it has become accepted in the literature (Fowler *et al.* 1985; Lotz *et al.* 1987; Wobig 1982) that diffusion coefficients are not well defined. Two more general confinement time calculations have been proposed, based respectively on an asymptotic test particle loss rate (Lotz *et al.* 1987) and on the decay rate of a functional of the test particle distribution (Garabedian 1989). We use both of these techniques later, and compare their results with D measurements. Details of the methods are given in Sections 3*a* and 3*b* below.

In 1993, Painter and Gardner calculated diffusion coefficients in H-1, using a Monte Carlo code (Painter 1993), over wide ranges of radial electric field, gyroradius, particle energy, and magnetic configuration. We have extended this work by allowing the possibility of finite beta plasmas (Fowler *et al.* 1985), by introducing new transport diagnostics (Garabedian 1989; Lotz *et al.* 1987), and by optimising the code for both parallel and vector computing environments. The code which we describe here has also been used to self-consistently calculate radial profiles of the radial electric field in the H-1NF Heliac (Dettrick *et al.* 1998*a*), in conditions of current experimental interest (Shats *et al.* 1996).

(2a) Equations of Motion

The code uses a gyro-averaged form for the drift velocity (Boozer and Kuo-Petravic 1981):

$$v_d = v_\parallel \frac{\mathbf{B}}{B} + \frac{mc}{eB}(v_\parallel^2 + \tfrac{1}{2}v_\perp^2)\frac{\mathbf{B}\times\nabla B}{B^2} + c\frac{\mathbf{B}\times\nabla\phi}{B^2} \, . \tag{1}$$

This can be expressed in Boozer straight-field-line coordinates (SFLC), for which the magnetic field satisfies

$$\mathbf{B} = \nabla\chi = \nabla\theta_0 \times \nabla\psi.$$

To use these coordinates we must assume that the magnetic field lines lie on a family of nonintersecting toroidal surfaces ('flux surfaces') which foliate the region of interest. The plasma surface depicted in Fig. 1 is such a flux surface, and the white lines on the surface represent magnetic field lines. In Boozer SFLC the radial coordinate is a flux surface label ψ, which corresponds to 2π times the toroidal flux enclosed by such a surface. The scalar potential θ_0 labels a magnetic field line on the surface and χ is proportional to the distance along that field line, so that together θ_0 and χ act as poloidal and toroidal 'angles' where, in toroidally symmetric geometry, a toroidal angle describes rotation about the central (straight) axis, while a poloidal angle describes local rotation about the magnetic (circular) axis. We refer to this (ψ, θ_0, χ) coordinate system, which does not have periodic angles, as 'rotating SFLC' because the position of $\theta_0 = 0$ follows a field line as it winds about the flux surface. We also use a periodic system of SFLC, which has the same radial coordinate, but with (periodic) poloidal and toroidal angles equal to $\theta = \theta_0 + \iota\phi$ and $\phi = (\chi - I\theta)/g$ respectively. Here $g = RB_\phi$ and $I = rB_\theta$ (Boozer and Kuo-Petravic 1981) are 2×10^{-7} times the poloidal current (in ampere) outside a flux surface and 2×10^{-7} times the toroidal current inside a flux surface, respectively (Fowler *et al.* 1985), where r and R are the minor and major radii of the torus.

SFLC have the advantage that many important plasma quantities are constant on a flux surface, so they can be parametrised in terms of a single coordinate, the flux surface label ψ. The convenience of such a parametrisation becomes obvious upon inspection of the complicated shape of the flux surface in Fig. 1. SFLC also remove the full $\mathbf{B}$ vector from the equations of motion, which can be expressed in terms of the magnetic field strength B (Fowler *et al.* 1985):

$$\dot{\psi} = (\dot{P}_\theta g - \dot{P}_\phi I)/\gamma, \tag{2}$$

$$\dot{\theta} = \left(\delta\frac{\partial B}{\partial\psi} + e\frac{\partial V}{\partial\psi}\right)\frac{\partial\psi}{\partial P_\theta} + \frac{e^2 B^2}{m}\rho_\parallel\frac{\partial\rho_\parallel}{\partial P_\theta}, \tag{3}$$

$$\dot{\phi} = \left(\delta\frac{\partial B}{\partial\psi} + e\frac{\partial V}{\partial\psi}\right)\frac{\partial\psi}{\partial P_\phi} + \frac{e^2 B^2}{m}\rho_\parallel\frac{\partial\rho_\parallel}{\partial P_\phi}, \tag{4}$$

$$\dot{\rho}_\parallel = [-(\rho_\parallel g' - \iota)\dot{P}_\theta + (\rho_\parallel I' + 1)\dot{P}_\phi]/\gamma, \tag{5}$$

where $\rho_{||} = mv_{||}/eB$ is the parallel gyroradius (parallel to the field line), the dots denote time derivatives, and the primes denote derivatives with respect to ψ. The functions γ and δ are defined by

$$\gamma = e[g(\rho_{||}I' + 1) - I(\rho_{||}g' - t)], \qquad \delta = e^2\rho_{||}^2 B/m + \mu\,,$$

where $\mu = mv_\perp^2/2B$, and the canonical momenta are

$$\dot{P}_\theta = -\delta\frac{\partial B}{\partial \theta}, \qquad \dot{P}_\phi = -\delta\frac{\partial B}{\partial \phi}.$$

We have finally,

$$\frac{\partial \psi}{\partial P_\theta} = \frac{g}{\gamma}, \qquad \frac{\partial \rho_{||}}{\partial P_\theta} = -\frac{\rho_{||}g' - t}{\gamma},$$

$$\frac{\partial \psi}{\partial P_\phi} = -\frac{I}{\gamma}, \qquad \frac{\partial \rho_{||}}{\partial P_\phi} = \frac{I'\rho_{||} + 1}{\gamma}.$$

The field strength B, the rotational transform t, and the currents g and I are calculated from formulae which have been predetermined by a plasma equilibrium code such as VMEC (Hirshman and Betancourt 1991). Except in the self-consistent calculations mentioned above (Dettrick *et al.* 1998*a*) the electrostatic potential V is usually specified using a model which assumes that there is no surface varying component, and that V is approximately parabolic in r, which is to say

$$V(\psi) = V_0(1 - \psi/\psi_{\mathrm{max}})\,, \tag{6}$$

where ψ_{max} is the radial coordinate at the plasma edge, and the magnitude of V_0 is typically equal to the value of T_i in electron volts.

(2b) Collision Operators

To model the pitch angle and energy scattering processes, the equations of motion for the pitch angle parameter $\eta = v_{||}/v$ and the energy $\mathcal{E}$ are formulated as stochastic differential equations, which are integrated using a weak, second order stochastic predictor-corrector method due to Platen (Kloeden and Platen 1992). This method was described, for pitch angle scattering, by Painter (1993).

To formulate the equations of motion in terms of stochastic differential equations, the stochastic (collision) process in each coordinate is decomposed into a drag (or drift) term a, and a dispersion (or diffusion) term b. Following Platen, the drag and dispersion terms in η are defined as

$$a(\eta_0) = \lim_{\Delta t \to 0} \frac{1}{\Delta t} \int_{-1}^{1} (\eta - \eta_0)f(\eta, t + \Delta t|\eta_0, t)d\eta, \tag{7}$$

$$b^2(\eta_0) = \lim_{\Delta t \to 0} \frac{1}{\Delta t} \int_{-1}^{1} (\eta - \eta_0)^2 f(\eta, t + \Delta t|\eta_0, t)d\eta, \tag{8}$$

where $f(\eta, t + \Delta t | \eta_0, t)$ is the probability of transition from η_0 to η in a time Δt for a test particle. That is, f is the probability distribution function for a test particle at time $t + \Delta t$, given that it was at η_0 at the earlier time t. The drag and dispersion terms in $\mathcal{E}$ are defined analogously. Following Painter, the probability distribution function is expanded in a Taylor series,

$$f(x, t + \Delta t | x_0, t) = \delta(x - x_0) + \frac{\partial f}{\partial t} \Delta t + O\{(\Delta t)^2\}, \tag{9}$$

where the delta function is involved because each test particle is treated separately, and each test particle is both monoenergetic and mono-directional. The time derivatives of the distribution functions are evaluated using the Lorentzian scattering operators from Boozer (Boozer and Kuo-Petravic 1981):

$$\frac{\partial f(\eta)}{\partial t} = \frac{\nu_p}{2} \frac{\partial}{\partial \eta}(1 - \eta^2) \frac{\partial f}{\partial \eta}, \tag{10}$$

$$\frac{\partial f(\mathcal{E})}{\partial t} = \frac{\partial}{\partial \mathcal{E}} \left[(2\mathcal{E} - T)\nu_{\mathcal{E}} f(\mathcal{E}) + 2\nu_{\mathcal{E}} T \mathcal{E} \frac{\partial f(\mathcal{E})}{\partial \mathcal{E}} \right]. \tag{11}$$

Substituting equation (10) into (9), and integrating the resulting equation (7) by parts, we obtain the drag coefficient,

$$a(\eta) = -\nu_p \eta. \tag{12}$$

Again substituting equation (10) into (9), but this time integrating equation (8) by parts, we obtain the dispersion coefficient,

$$b(\eta) = \sqrt{\nu_p(1 - \eta^2)}. \tag{13}$$

For the energy coordinate, the analogous substitutions are made using equation (11) instead of (10), and we arrive at the drag and dispersion terms

$$a(\mathcal{E}) = -2\nu_{\mathcal{E}} \left(\mathcal{E} - \tfrac{3}{2}T - \frac{\mathcal{E}T}{\nu_{\mathcal{E}}} \frac{\partial \nu_{\mathcal{E}}}{\partial \mathcal{E}} \right), \tag{14}$$

$$b(\mathcal{E}) = 2\sqrt{\mathcal{E}T\nu_{\mathcal{E}}}, \tag{15}$$

which are equivalent to the Monte Carlo operators given by Boozer and Kuo-Petravic. The drag coefficient tends to relax the distribution toward the thermal energy, while the dispersion coefficient tends to 'thermalise' the energy distribution. Under the influence of these two terms only, an arbitrary initial distribution will relax to a Maxwellian, of temperature T.

(2c) Stochastic Differential Equations

To complete the stochastic differential equation formulation using Platen's prescription, the collisional drag and dispersion coefficients are combined with equations (2)–(5) above:

$$d\psi = \left[(\dot{P}_\theta g - \dot{P}_\phi I)/\gamma \right] dt, \tag{16}$$

$$d\theta = \left[\left(\delta \frac{\partial B}{\partial \psi} + e \frac{\partial V}{\partial \psi} \right) \frac{\partial \psi}{\partial P_\theta} + \frac{e^2 B^2}{m} \rho_{||} \frac{\partial \rho_{||}}{\partial P_\theta} \right] dt, \tag{17}$$

$$d\phi = \left[\left(\delta \frac{\partial B}{\partial \psi} + e \frac{\partial V}{\partial \psi} \right) \frac{\partial \psi}{\partial P_\phi} + \frac{e^2 B^2}{m} \rho_{||} \frac{\partial \rho_{||}}{\partial P_\phi} \right] dt, \tag{18}$$

$$d\rho_{||} = \left[[-(\rho_{||} g' - \iota)\dot{P}_\theta + (\rho_{||} I' + 1)\dot{P}_\phi]/\gamma - \nu_p \rho_{||} \right] dt$$

$$+ \sqrt{\nu_p \frac{mv}{eB}(1 - \eta^2)} dW_1, \tag{19}$$

where the dW_1 are stochastic analogues (Kloeden and Platen 1992) of the time increments dt:

$$dW_1 = \begin{cases} -\sqrt{3dt}, & 0 \le p < \frac{1}{6} \\ \sqrt{3dt}, & \frac{1}{6} \le p < \frac{1}{3} \\ 0, & \frac{1}{3} \le p < 1, \end{cases}$$

where $p \in [0, 1)$ is a random number.

When only pitch angle scattering is used in the code, which is the usual case, the test particle energy is relaxed with the same time constant as is used in the pitch angle scattering (Lotz *et al.* 1987):

$$d\mathcal{E} = \nu_p(\mathcal{K}_0 - \mathcal{K})dt, \tag{20}$$

where $\mathcal{K}_0$ is the initial kinetic energy for each particle. This is to stop collisionless, electrostatic confinement from dominating the transport which is measured in the code. When energy scattering is included, the increment in the energy coordinate is

$$d\mathcal{E} = -2\nu_\mathcal{E} \left(\mathcal{E} - \frac{3}{2} T - \frac{\mathcal{E}T}{\nu_\mathcal{E}} \frac{\partial \nu_\mathcal{E}}{\partial \mathcal{E}} \right) dt + 2\sqrt{\mathcal{E}T\nu_\mathcal{E}} dW_2, \tag{21}$$

where dW_2 is defined by (Kloeden and Platen 1992)

$$dW_2 = \begin{cases} -dt, & 0 \le p < \frac{1}{2} \\ dt, & \frac{1}{2} \le p < 1 \end{cases}$$

where $p \in [0, 1)$ is a random number.

Usually, energy scattering is not used, because it increases the simulation times by up to an order of magnitude, without significantly affecting the results (Lotz and Nührenberg 1988).

(2d) Collision Frequencies

For an ensemble of particles of species a streaming through a background plasma composed of species b, the expected rate of increase of spread in the velocity component transverse to the original direction is (Takizuka and Abe 1977):

$$\langle dv_{a\perp}^2/dt \rangle = \nu_d^{ab} v_a^2, \tag{22}$$

and the expected rate of increase of the energy spread is

$$\langle d(\Delta E_a)^2/dt \rangle = \nu_E^{ab} E_a^2. \tag{23}$$

Here ν_d^{ab} and ν_E^{ab} are given by

$$\nu_d^{ab} = \nu_0^{ab} \left[\Phi(x_{ab}) - (\Phi(x_{ab}) - x_{ab}\Phi'(x_{ab}))/2x_{ab}^2 \right] ,$$

$$\nu_E^{ab} = 2\nu_0^{ab}(\Phi(x_{ab}) - x_{ab}\Phi'(x_{ab}))m_a/m_b,$$

where the sub or superscript ab denotes a quantity which applies to a particle of species a streaming through a background composed of species b. There is no implied summation over the a and b indices. The variable $x_{ab} = (m_b\mathcal{K}_a/m_a T_b)^{\frac{1}{2}}$ is the normalised velocity ($\mathcal{K}_a$ is the kinetic energy of the particle of species a). Here Φ is the well known error function,

$$\Phi(x) = \frac{2}{\sqrt{\pi}} \int_0^x \exp(-t^2)dt \,,$$

and the characteristic scattering frequency ν_0^{ab} is (Book 1990)

$$\nu_0^{ab} = 4\pi e_a^2 e_b^2 \lambda_{ab} n_b / m_a^2 v_b^3 \,,$$

where λ_{ab} is the Coulomb logarithm.

In the SDE formulation described in Section 2c above, we use the definitions

$$\nu_p = (\nu_d^{aa} + \nu_d^{ab})/2, \qquad \nu_{\mathcal{E}} = (\nu_E^{aa} x_{aa}^2 + \nu_E^{ab} x_{ab}^2)/4$$

in the code by substituting them into equations (19) and (21). Velocity space scattering simulations (i.e. simulations with no magnetic field geometry) then demonstrate excellent agreement with the theoretically expected relaxation rates of equations (22) and (23). Fig. 3 shows the results of these simulations where an ensemble of monoenergetic and monodirectional test particles were scattered off a background plasma of ions and electrons using the SDE method. For this
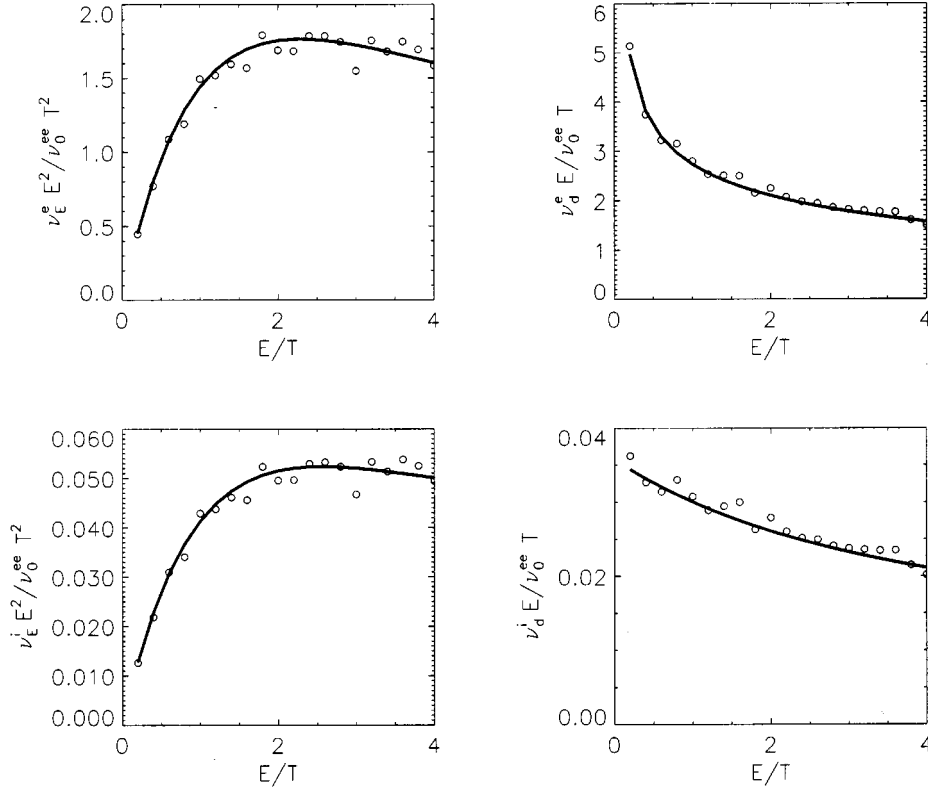
Fig. 3. Comparison of normalised relaxation rates of energy (left) and perpendicular velocity (right), between theory (curves) and the results of Monte Carlo velocity space simulations (circles), for electrons streaming through a background of ions and electrons (top row), and ions streaming through a background of ions and electrons (bottom row).

figure the relaxation rates $\nu_E^a = \nu_E^{ab} + \nu_E^{aa}$ and $\nu_d^a = \nu_d^{ab} + \nu_d^{aa}$ of the test particle energy and velocity distributions were calculated from equations (22) and (23).

3. Transport Measurements

(3a) Diffusion Coefficients

In test-particle Monte Carlo codes the radial diffusion D is estimated from the average rate of change of the radial variance of the test particle distribution. We use a diffusion coefficient estimator which combines Painter's method, which correctly accounts for particles lost during the simulation, with that of Fowler *et al.*, which incorporates a 'quiet start' to reduce the effect of initial non-diffusive processes. The resulting diffusion coefficient estimator is

$$D = \frac{a_p^2}{2} \frac{\displaystyle\sum_i [(r_{2i} - \overline{r_2})^2 - (r_{1i} - \overline{r_1})^2]}{\displaystyle\sum_i t_i}, \tag{24}$$

where a_p is the plasma minor radius, the overbar denotes the average over the test particle distribution, and the index i runs over all test particles including those which were lost. The r_{1i} are the radial positions of the particles at the end of the quiet start phase (at the beginning of the collisional phase), and the r_{2i} are the positions when the diffusion coefficient is calculated. At the beginning of the quiet start phase, the test particles are distributed uniformly on a single flux surface, and are distributed uniformly in the pitch angle parameter, $\eta = v_{||}/v$. For confined particles, $t_i = \tau_{\mathrm{sim}}$, and for lost particles, t_i is the time when the plasma boundary, $r = 1$, was crossed.

If τ_{orb} is the time a particle takes to make a toroidal orbit, τ_{90} is the characteristic time of the collision process, and τ_{conf} is the confinement time, then the simulation time τ_{sim} should satisfy

$$\tau_{\mathrm{orb}}, \tau_{90} < \tau_{\mathrm{sim}} < \tau_{\mathrm{conf}}, \tag{25}$$

to ensure that the effects of the magnetic geometry and the collisional processes are properly incorporated, and that most of the test particles are retained in the calculation.

(3b) Confinement Time

We consider two estimations of confinement time. In the first, due to Lotz *et al.* (1987), the test particles are propagated in the background fields as described above excepting that lost particles are replaced by duplicating one of the confined test particles. The index of the test particle to be duplicated is calculated from the cyclic relationship

$$n_{\mathrm{dup}}^i = (n_{\mathrm{dup}}^{i-1} + k_{\mathrm{cyc}}) \bmod N,$$

where the last particle duplicated has index n_{dup}^{i-1}, N is the number of test particles in the simulation, and k_{cyc} is relative prime to N. The procedure continues until a steady state is achieved, at which point the inverse of the MC replenishment rate is the confinement time, τ_{L}.

The second estimation of confinement time, due to Garabedian (1989) calculates the exponential decay constant, τ_{G}, of a functional, $H(t) \sim \exp(-t/\tau_{\mathrm{G}})$, of the test particle distribution:

$$H(t) = \frac{1}{N} \sum_j (1 - s_{0k}) \cos\left(\frac{\pi}{2} \frac{s_{1j} - s_{0k}}{1 - s_{0k}s_{1j}}\right), \tag{26}$$

where N is the total number of test particles and s, a radial coordinate, is the toroidal flux enclosed by a flux surface, normalised to 1 at the last closed flux surface. The N test particles are initialised simultaneously on eight flux surfaces (with $N/8$ particles per surface), which have radial positions s_{0k}, and the $s_{1j}(t)$ denote the subsequent positions of the test particles at time t. For this method the simulation time should meet the criterion in equation (25).

(3c) Exponential Decay Time

To put the confinement time calculations into some perspective, we have also calculated the exponential decay constant of the particle distribution. For this purpose, N_0 test particles were initialised with a parabolic radial distribution in the plasma, and were propagated, with no particle source terms, until N_0/e test particles were left. During this time, we recorded the logarithm of the number of confined test particles, $\log N_1(t)$. When $\log N_1(t)$ is linear in time, the time-gradient gives the exponential decay constant, τ_e.

4. Comparative Results

In this section we present our results using the mean free path and loss rate normalisations introduced by Lotz and Nührenberg (1988), where the normalised mean free path L_* is given by $L_* = L_{\mathrm{mfp}}/L_c$, with $L_{\mathrm{mfp}} = v\tau_{90}$ and $L_c = \pi R_0/\ell$, and the dimensionless diffusion coefficient D_* is $D_* = D/D_p$, where D_p is the tokamak plateau value $D_p = 0 \cdot 64\rho^2 v/\ell^2 L_c = 0 \cdot 64\rho^2 v/\ell\pi R_0$. Here, v is the particle velocity and $\rho = mv/eB_0$ is the formal gyroradius, where B_0 is the magnetic field strength at the magnetic axis. The normalised loss rate, $S_* = S/S_p$, is calculated using the analogous plateau loss rate, $S_p = D_p\left(2 \cdot 4/a_p\right)^2$.

We begin by benchmarking the code against a well-known analytic tokamak model. All subsequent calculations are performed for a 200 eV hydrogen plasma, in H-1NF in a 1T field, in the standard magnetic configuration. These conditions may be attainable in the H-1 Heliac when the National Facility upgrade is complete.

(4a) Tokamak Benchmark

To benchmark the code against an analytic model, we calculated the diffusion coefficient and the three decay times described above, for the same tokamak test case that was studied by Fowler *et al*. We used their analytic model for the tokamak diffusion coefficient, which is derived from the general expressions of Hinton and Hazeltine (1976). The test case parameters were $B = 2$ T, $R_0 = 2$ m, $a_p = 0 \cdot 2$ m, $\ell = 0 \cdot 5$, and $T_i = T_e = 1000$ eV. The mean free path was varied via the density, and the radial electric field was zero for each calculation. In Fig. 4, Monte Carlo results are calculated using both monoenergetic ($\mathcal{E}/T_i = 1 \cdot 5$) test particle distributions ($\triangle$, $+$, $\times$, and $\bullet$) and Maxwellian distributions ($\square$ and $\ast$). As has been found previously (Lotz and Nührenberg 1988), the monoenergetic and Maxwellian results coincide closely.

(4b) Comparison between τ Methods

We show in Fig. 5 the loss rates for H-1NF which are obtained using the three methods. Results are shown for two radial electric fields, which are specified using the values $V_0 = -T_i$ and $V_0 = 0$, in equation (6).

In Fig. 5 there is good agreement between the τ_{G} method ($\times$) and τ_{L} method ($+$), when the electric field is zero, but when E_r is finite and the mean free path is not long ($L_* \lesssim 30$), the agreement breaks down. We interpret this as follows: in the intermediate mean free path regime, the transport is mainly diffusive, so the loss rate is a function of the density gradient. In Lotz's method, the asymptotic test particle density gradient is a function of the electric field
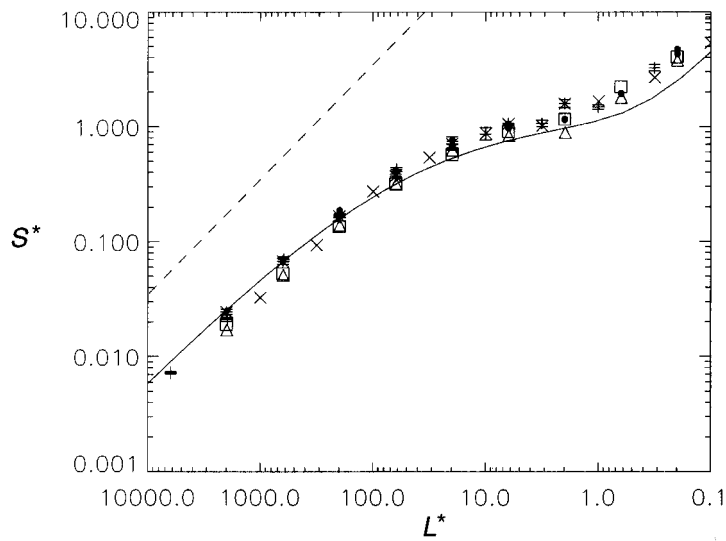
Fig. 4. Comparison of normalised tokamak loss rates, calculated from D ($\triangle$, monoenergetic, and $\square$, Maxwellian) from $1/\tau_L$ ($+$, monoenergetic, and $*$, Maxwellian), from $1/\tau_G$ ($\times$, monoenergetic) and from $1/\tau_e$ ($\bullet$, monoenergetic). The solid curve is the analytic result, and the dashed line represents the loss rate at which $\tau_{90} = \tau_{conf}$.

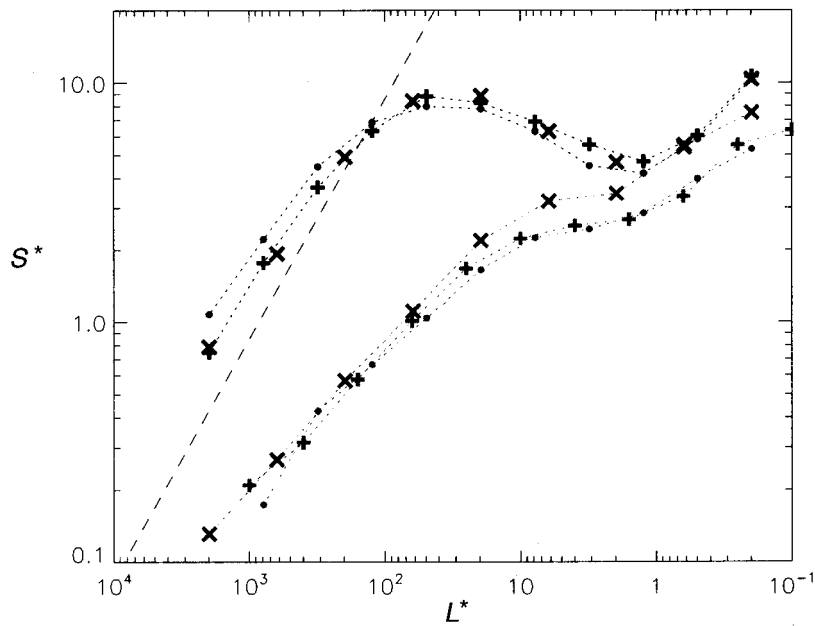**Fig. 5.** Normalised loss rates in H-1NF, calculated using Lotz's technique ($+$), Garabedian's technique ($\times$), and the direct loss rate ($\bullet$), for two electric fields, specified by $V_0 = -T_i$ (two lower curves) and $V_0 = 0$ (two upper curves). The diagonal dashed line represents the loss rate at which $\tau_{90} = \tau_{conf}$. Values throughout are $T_i = 200$ eV and $B_0 = 1$ T.

(Lotz *et al.* 1987), but in Garabedian's method, the effective density gradient is independent of E_r, since it is determined by the envelope of the function $H(t)$, of equation (26). Therefore the results differ for intermediate mean free paths. In the long mean free path regime ($L_* \gtrsim 30$), the loss rate is not determined by the density gradient but by direct particle losses, so the τ_G and τ_L results are in agreement.

The figure also demonstrates that the τ_e method ($\bullet$) has fair agreement with the τ_L method ($+$) throughout. This agreement is at its best when $\tau_{\rm conf} \gg \tau_{90}$ (to the right of the dashed diagonal line) because the collisions have time to replenish the loss cone before it is significantly depleted, so the (decaying) test particle distribution in the τ_e method is in a state which is close to the asymptotic state arrived at using Lotz's technique.
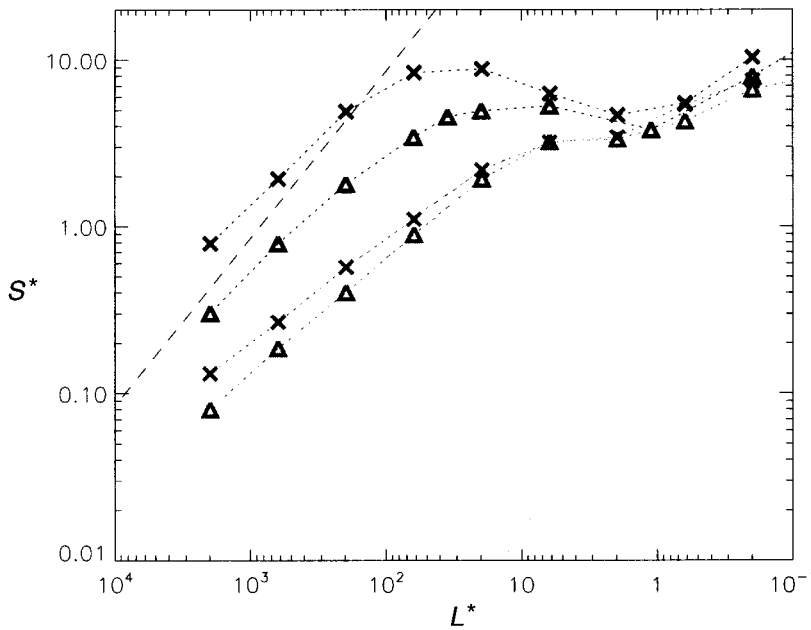

Fig. 6.   Normalised loss rates in H-1NF, calculated using Garabedian's technique ($\times$) and the diffusion coefficient ($\triangle$), for two electric fields, specified by $V_0 = -T_i$ (two lower curves) and $V_0 = 0$ (two upper curves).

(4c) Comparison between τ_G and D

In Fig. 6 we compare the results for the diffusion coefficient D calculated from equation (3), and $1/\tau_G$ for the same conditions as in the previous section. Best agreement is found at $L_* \approx 1$, where diffusive transport dominates. Poor agreement is found elsewhere, when it is expected that convective losses driven by diffusion in velocity space will dominate. However, in these conditions it is difficult to compare the two calculations, since the S_* normalisation method is based around the consideration of diffusion in a straight cylinder, rather than in a helical toroid. In the short mean free path regime, where the device geometry is not so important, the comparisons are more meaningful.

(4d) D at Short Mean Free Path

The diffusion coefficient is often considered to be insensitive to the electric field at short mean free path, with many authors assuming that the stellarator diffusion coefficient will become equal to the tokamak diffusion coefficient, when $L_* \ll 1$. Examples which contradict this assumption have been found using the DKES code (Solano *et al.* 1988) and another Monte Carlo code (Potok *et al.* 1980). To look for this effect in H-1NF, we have extended our D results into the short mean free path regime in Fig. 7. Only negative electric fields (this time $V_0 = 0$, -1 and -2) were simulated, since positive ambipolar fields are only expected in the long mean free path regime. The results show qualitative agreement with the results given by Solano and by Potok.
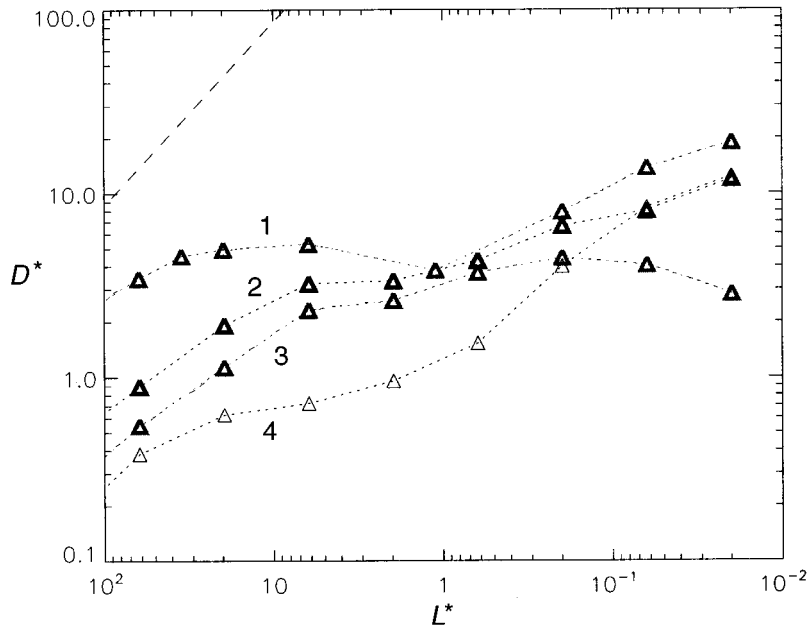

Fig. 7. Normalised diffusion coefficients in H-1NF, at short mean free path, for electric fields specified by $V_0 = 0$ (curve 1), $V_0 = -T_i$ (curve 2) and $V_0 = -2T_i$ (curve 3). Curve 4 corresponds to a tokamak of similar dimensions. The diagonal dashed line represents the loss rate at which $\tau_{90} = \tau_{\mathrm{conf}}$. Values throughout are $T_i = 200$ eV and $B_0 = 1$ T.

The dependence of D on E_r in the short mean free path regime can be explained within the Monte Carlo framework since, when $L_* \ll 1$, the usual notions of passing and trapped orbits lose their meaning, so the transport is determined by an effective time-average over many short-lived orbit states. In such a scenario, the transport can be expected to depend on the average value of v_r/v (v_r is the radial component of the drift velocity), which is diminished by large radial electric fields.

5. Computing Considerations

The test particle distribution must adequately sample both the magnetic field geometry and the velocity phase space regions over the course of its trajectory.

Because of this, the CPU time required by the calculation depends strongly on the complexity of the magnetic geometry. To ensure that sampling is adequate, we used a large number of test particles ($N_p \sim 10^3$) for the D, τ_G and τ_e method calculations, and followed the test particle orbits for a period τ_{sim}, which was typically $3 \max(\tau_{90}, \tau_{orb})$. Because the τ_L method requires longer simulation times ($\tau_{sim} \gg 10$) in order to arrive at the asymptotic test particle distribution, a smaller test particle population ($N_p \sim 100$) is sufficient for good Monte Carlo statistics. Because the test particles do not interact, the code is suitable for vectorisation and parallelisation, so a Multiple-Processor, Multiple-Data parallel algorithm was developed to efficiently implement this calculation on distributed computing architectures.

An adaptive timestep length is used for the integration, so it is not obvious how the CPU time will scale with collisionality. We plot it in Fig. 8, where we see that the CPU time scales unfavourably in the long-mean-free-path regime for the τ_G method ($+$) and scales unfavourably in the short-mean-free-path regime for the τ_L method ($\times$).

For the τ_L method, the simulation continues until an asymptotic state is obtained. The CPU time is most favourable in the long-mean-free-path regime (where the D and τ_G methods have poor CPU scaling), and when the electric field is small or positive. The CPU times can be reduced for the Lotz method by initialising the radial test particle distribution with a guess at the eventual asymptotic state: a (typically) parabolic radial distribution of test particles.
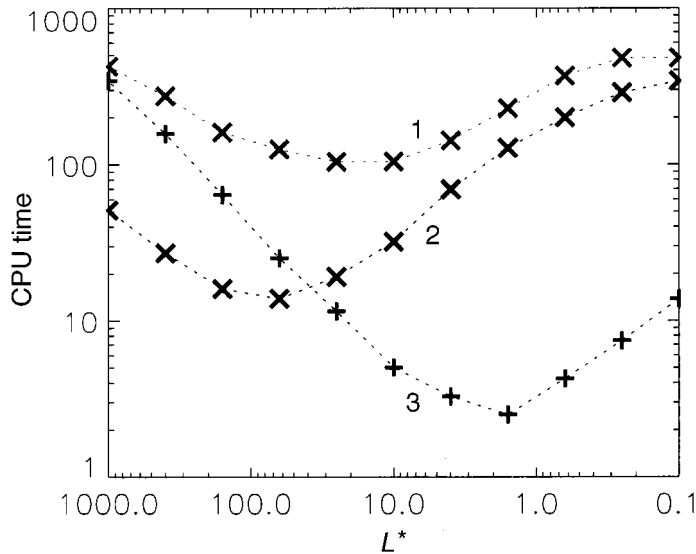

Fig. 8. Computing time in seconds versus mean free path for the Garabedian method (curve 3) and the Lotz method. Two cases are shown for the Lotz method: H-1NF with no electric field (curve 2) and H-1NF with $V_0 = -T_i$ (curve 1).

6. Discussion

We have compared the results of three methods for the calculation of the confinement time, and have found good agreement in the long-mean-free-path

regime in H-1NF. In the intermediate mean free path regime, we find fair agreement between τ_e and τ_L, and poor agreement between τ_L and τ_G. We attribute this to the role that the density gradient plays in determining the loss rate when the transport is mainly diffusive. Of the three methods, we prefer the one due to Lotz, since it simultaneously generates an equilibrium loss rate and an asymptotic test particle distribution function (Lotz *et al.* 1987; Lotz and Nührenberg 1988). Also, in stellarators Lotz's method has favourable CPU scaling in the long mean free path regime.

One advantage of calculating the confinement time is that this is the quantity which is most readily measured in experiment, so direct comparison between simulations and experiment is possible. In contrast, comparison of a computed diffusion coefficient with experimental results usually requires some intermediate theoretical interpretation. The diffusion coefficient method has the advantage that it is computationally efficient in the intermediate and short mean-free-path regimes, and also it calculates a transport coefficient which is not influenced by the density profile, except via the collision frequency. As a result, D is more appropriate for the fitting of analytic models to the MC results, as was done by Painter and Gardner. Such analytic models are important for studies of transport, because they are capable of closely reproducing the Monte Carlo results, over a wide range of physical conditions, in a very small fraction of the MC computing time. We have verified a previous result of the DKES code in TJ-II (Solano *et al.* 1988), that the diffusion coefficient is sensitive to strong radial electric fields in the high collision frequency regime. An implication of this is that the model fitting performed by Painter and Gardner must be re-evaluated in order to be applicable to this regime.

7. Conclusion

In this paper, we have described and benchmarked a Monte Carlo transport code, and used it to compare some of the Monte Carlo transport diagnostic techniques which can be found in the literature. We have not performed a detailed transport study in H-1NF, rather, our objective has been to come to a better understanding of the Monte Carlo model.

The Monte Carlo code has been successfully benchmarked in both tokamak and H-1NF magnetic fields, and has been used to compare some of the Monte Carlo transport diagnostics from the literature. Of the confinement time methods we studied, we prefer the one due to Lotz, which simultaneously generates an equilibrium loss rate and an asymptotic test particle distribution function. A Multiple-Processor, Multiple-Data parallel algorithm was developed to efficiently implement this calculation on distributed computing architectures. A diffusion coefficient estimator due to Painter has also been described in some detail, and was used to verify in H-1NF a result which was obtained by Solano *et al.* using the DKES code: at collision frequencies much higher than the tokamak plateau collision frequency, the diffusion coefficient is a function of the radial electric field.

References

Book, D. L. (1990). 'NRL Plasma Formulary', NRL Publication No. 177–4405 (Naval Research Laboratory: Washington, DC).

Boozer, A. H., and Kuo-Petravic, G. (1981). *Phys. Fluids* **24**, 851.

Dettrick, S. A, Gardner, H. J., and Dewar, R. L. (1998*a*). *J. Plasma Fusion Res. Series (Proc. ISC-11 and ITC-8)* **1**, 222.

Dettrick, S. A., Lloyd, S. S., Gardner, H. J., and Dewar, R. L. (1998*b*). *Nucl. Fusion* **38**, 1001.

Dewar, R. L., and Hudson, S. H. (1997). *Physica* D **112**, 275.

Fowler, R. H., Rome, J. A., and Lyon, J. F. (1985). *Phys. Fluids* **28**, 338.

Garabedian, P. R. (1989). *SIAM Review* **31**, 542.

Hinton, F. L., and Hazeltine, R. D. (1976). *Rev. Mod. Phys.* **48**, 239.

Hirshman, S. P., and Betancourt, O. (1991). *J. Comput. Phys*. **96**, 99.

Kloeden, P. E., and Platen, E. (1992). 'Numerical Solution of Stochastic Differential Equations', Applications of Mathematics Series Number 23 (Springer: Berlin).

Lotz, W., and Nührenberg, J. (1988). *Phys. Fluids* **31**, 2984.

Lotz, W., Nührenberg, J., and Schluter, A. (1987). *J. Comput. Phys*. **73**, 73.

Mynick, H. E. (1982). *Phys. Fluids* **25**, 325.

Painter, S. L. (1993). *Comput. Phys. Commun.* **77**, 342.

Painter, S. L., and Gardner, H. J. (1993). *Nucl. Fusion* **33**, 1107.

Potok, R. E., Politzer, P. A., and Lidsky, L. M. (1980). *Phys. Rev. Lett.* **45**, 1328.

Shats, M. G., Rudakov, D. L., Blackwell, B. D., Borg, G. G., Dewar, R. L., Hamberger, S. M., Howard, J., and Sharp, L. E. (1996). *Phys. Rev. Lett.* **77**, 4190.

Solano, E. R., Rome, J. A., and Hirshman, S. P. (1988). *Nucl. Fusion* **28**, 157.

Takizuka, T., and Abe, H. (1977). *J. Comput. Phys.* **25**, 205.

Wobig, H. (1982). *Z. Naturforsch.* **37a**, 906.